Sensors and Actuators A 188 (2012) 389–395

Contents lists available at SciVerse ScienceDirect

Sensors and Actuators A: Physical

journal homepage: www.elsevier.com/locate/sna

Power enhancement of micro thermoelectric generators by microfluidic heat transfer packaging

N. Wojtas[a,*], E. Schwyter[a,b], W. Glatz[b], S. Kühne[a], W. Escher[c], C. Hierold[a]

[a] Micro and Nanosystems, ETH Zurich, Tannenstrasse 3, 8092 Zurich, Switzerland
[b] greenTEG GmbH, Tannenstrasse 3, 8092 Zurich, Switzerland
[c] Zurich Research Laboratory, IBM Research, Säumerstrasse 4, 8803 Rüschlikon, Switzerland

ARTICLE INFO

Article history:
Available online 29 December 2011

Keywords:
Thermoelectric power generation
Micro heat transfer systems
Microfluidic packaging
Thermal coupling

ABSTRACT

This paper reports on the design, fabrication and proof of concept of a multilayer fluidic packaging system enabling an increase in the output power performance of micro thermoelectric generators (μTEGs). The complete integration of the microfluidic heat transfer system (μHTS) with a μTEG is successfully demonstrated.

The fabricated prototype is characterized with respect to its thermal and hydrodynamic performance as well as the generated output power. At a very low pumping power of 0.073 mW/cm^2, a heat transfer resistance of 0.74 cm^2 K/W is reached. The assembled device generated up to 1.47 mW/cm^2 at an applied temperature difference of 50 K and a fluid flow rate of 0.1 l/min. Further system improvements and the potential of the proposed packaging approach are discussed.

1. Introduction

With significant improvements in the figure of merit (ZT) of thermoelectric materials [1,2] and the potential of large scale production [3], thermoelectric energy harvesting is becoming promising for commercial applications. Recovered waste heat from industrial equipment, automotives or home appliances can be used to power a variety of systems, such as wireless sensor nodes [4], car electronics [5] or small consumer applications.

Efficient thermoelectric power generation, however, requires not only a high performance TEG but also a complete system optimization including thermal coupling to the hot and cold side reservoir. The output power of a generator scales with the square of the applied temperature gradient across the TEG. In order to maintain this thermal gradient, efficient heat dissipation and supply are essential, in particular for thin μTEGs.

The most common approaches to maintain a thermal gradient across a TEG are the integration of passive heat spreaders or conventional large scale fluidic heat exchangers [6]. The first solution has the advantage of not requiring an active cooling medium, but suffers from high heat transfer resistance and thus insufficient heat transfer. Large scale fluidic heat exchangers have an improved thermal performance, but also consume much pumping power due to high fluid flows.

A more effective approach to enhance the thermal coupling to the hot and cold reservoirs is to increase the convective surface area by using heat transfer systems on the micrometer scale [7]. Another approach is to reduce the interfacial thermal losses by direct integration of heat transfer systems (HTSs) into the packaging [8].

Many efficient solutions for active surface cooling in the micrometer range have been developed for integrated circuits and optoelectronic devices. The system designs and methods include simple microchannels [9], multilayer manifold structures [10–12], porous media [13] and jet impingement [14]. While most devices exhibit a similar heat dissipation capacity, manifold structures in particular show a superior hydrodynamic performance [7].

A representative comparison of the impact of different heat dissipation systems on the output performance of a Bi_2Te_3 μTEG ($Z = 1.1 \times 10^{-3}$ K^{-1}) is depicted in Fig. 1. The heat dissipation system performance is characterized by its heat transfer resistance R_{HS}. The μTEG output power is simulated as a function of different thermal coupling to the cold side reservoir (T_0) and a varying heat source temperature (T_{HOT}). The applied model consists of a TEG model with matched electrical load [15] extended with an attached heat transfer resistance, R_{HS}. Fig. 1 shows that a significant increase in the output power can be achieved by reducing the heat transfer resistance. Therefore, combining μTEGs with low pumping power microfluidic HTS will result in a substantial output power enhancement.

* Corresponding author at: Micro and Nanosystems, ETH Zurich, CLA J11.1, Tannenstrasse 3, CH-8092 Zurich, Switzerland. Tel.: +41 44 632 4899; fax: +41 44 632 1462.
E-mail address: wojtas@micro.mavt.ethz.ch (N. Wojtas).

0924-4247/$ – see front matter © 2012 Elsevier B.V. All rights reserved.
doi:10.1016/j.sna.2011.12.043

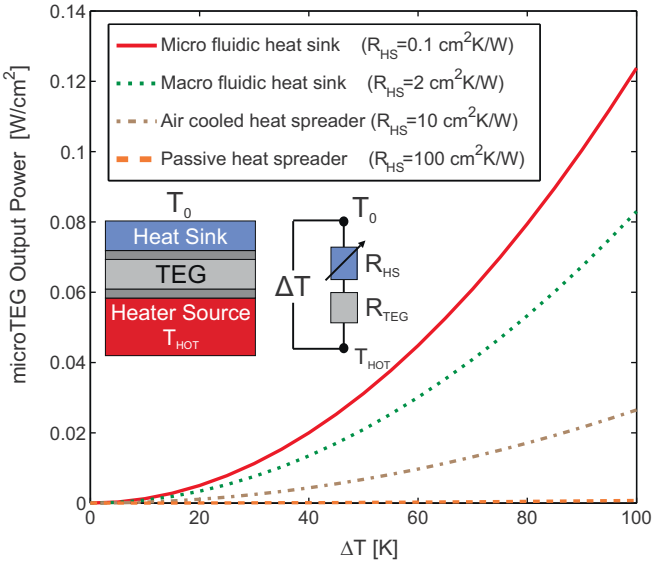

Fig. 1. Simulated Bi_2Te_3 μTEG ($Z = 1.1 \times 10^{-3}$ K^{-1}, $R_{TEG} = 5.9$ cm^2 K/W), output power dependence on different attached heat transfer systems on the cold side with representative values of heat transfer resistances (R_{HS}). The cold side temperature is fixed to $T_0 = 300$ K. A perfect heat transfer between T_{HOT} and the μTEG was assumed. The figure inset shows the schematics of the simulated setup and its equivalent thermal circuit.

Potential application fields of μTEGs with fluidic heat dissipation and supply would range from automotive systems to industrial processes, where cold as well as warm fluids are available.

The presented packaging approach enables the integration of a multilayer fluidic μHTS by directly bonding it onto the μTEG surface. In Fig. 2a, an exploded view of the μTEG/μHTS stack is depicted and Fig. 2b shows the assembled device. The packaging system consists of a high aspect-ratio copper microchannel layer as the heat transfer structure and a polymeric manifold layer. The manifold layer homogenously distributes the liquid through the inlet slots into the lower microchannels and collects it at the outlet slots, as schematically shown in Fig. 2c. For a constant pressure drop over the entire channel length, the manifold channels are tapered. This

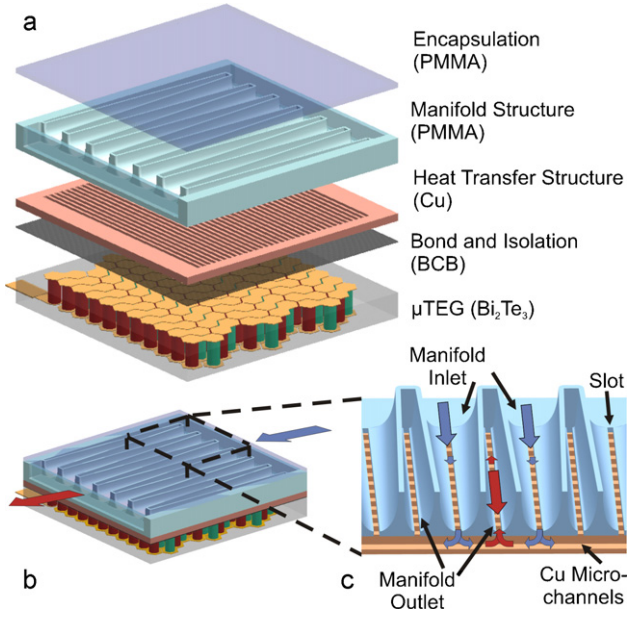

Fig. 2. Exploded view of the μHTS and μTEG multilayer stack (a). Assembled system (b) and cross section view showing the fluid path (c).

two-layer configuration results in very short fluid paths inside the microchannels, ensuring uniform cooling and small pressure losses [10]. In particular, the reduced hydrodynamic resistance offers a significant advantage over conventional one layer heat sinks, since the necessary pumping power needs to be subtracted from the μTEG output power for an overall system performance evaluation. Additionally, low heat transfer resistances and thus high heat fluxes are enabled by the high aspect-ratio copper microchannels and the thin interface bond layer between μHTS and μTEG (Fig. 2a). A further system improvement is achieved by choosing a thermally isolating polymer as the manifold material. This limits the thermal crosstalk between the manifold and the copper channels and therefore the heating up of the inlet fluid.

In this work, the fabrication process of two layer μHTSs and their integration with μTEGs is presented. A fabricated μHTS is first analyzed with respect to its heat transfer and hydrodynamic performance. In a second step, a μHTS device is integrated with a μTEG and the thermoelectric Seebeck voltage is measured as a function of the applied fluid flow rate and temperature gradient. Based on the measurement results, the influence of the μHTS to μTEG thermal resistance ratio as well as the potential performance improvement of the microfluidic package approach is discussed.

2. Fabrication process

The two functional layers of the μHTS, the microchannel and manifold structure, respectively, are fabricated in separate processes and assembled on chip level. For the microchannel fabrication, an SU-8 based LIGA (Lithography, Electroplating, and Molding) process was used, allowing for high aspect ratios [16,17], batch fabrication and low cost electrochemical metal deposition. The process flow is illustrated in Fig. 3. In the first step, 1 μm of lift-off resist (LOR) is spin coated on the wafer for a later release of the microchannels from the support. Next, a copper seed layer (1 μm) and a chromium adhesion layer (10 nm) are deposited by e-beam evaporation. The prepared seed wafer is coated with a 200 μm thick SU-8 3050 film. To improve the layer thickness homogeneity, the spin coating is performed in two steps of 100 μm and an edge bead removal is carried out. In the subsequent photolithography (Fig. 3a), long cooling and additional relaxation times are added for stress reduction in the SU-8. Due to the high aspect ratio and length of the mold structures, a reduced intrinsic stress level of SU-8 is crucial for the adhesion to the substrate. The structures are developed in ultrasound in order to improve convection inside the high aspect ratio trenches. The copper microchannels are grown by electrochemical deposition with an applied current density of 3 A/dm^2 (Fig. 3b). The mold is overgrown in order to form the base of the microchannels. After a top surface planarization by mechanical polishing, the wafer is released from the support and separated into 8 mm × 8 mm chips. The seed layer peels off during the release process. Finally, the SU-8 mold is removed by chemical etching (Fig. 3c).

The microchannels are bonded to the μTEG (the basic μTEG fabrication process is reported in [3]) by an 8 μm benzocyclobutene (BCB) adhesion layer (Fig. 3d). The bonding is performed at a low temperature of 423 K for 16 h and a tool pressure of 30 kPa in order not to damage the μTEG. The PMMA manifold distribution channels are fabricated by micromilling and encapsulated by γ-butyrolactone (GBL) solvent bonding of a 250 μm PMMA foil. A 10 μm thin double-sided adhesive tape is laminated to the manifold, and the connecting slots at the bottom of the manifold structure (see Fig. 2c) are opened by micro laser milling (Fig. 3e). Finally, the manifold is mounted onto the microchannel and the μTEG stack (Fig. 3f).

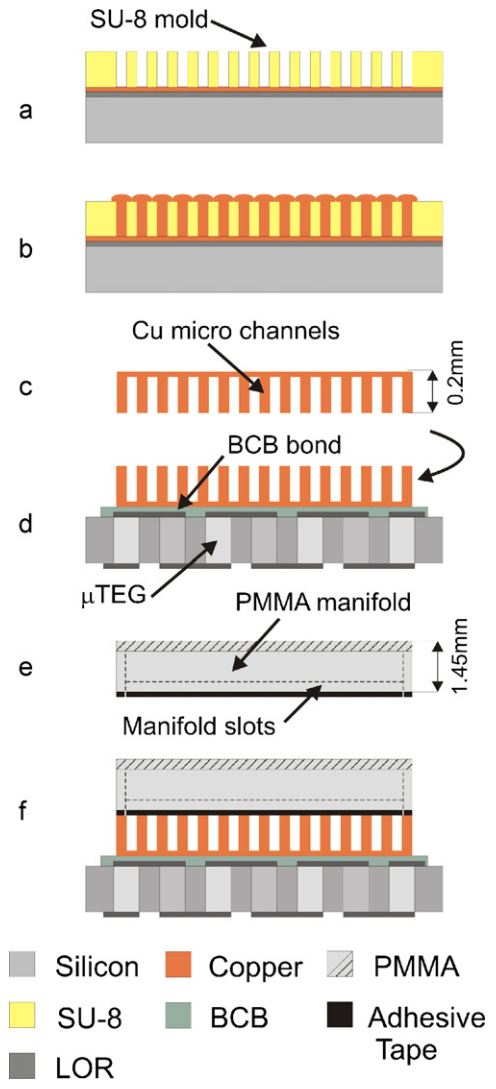

Fig. 3. Fabrication process flow of the μHTS/μTEG multilayer stack.

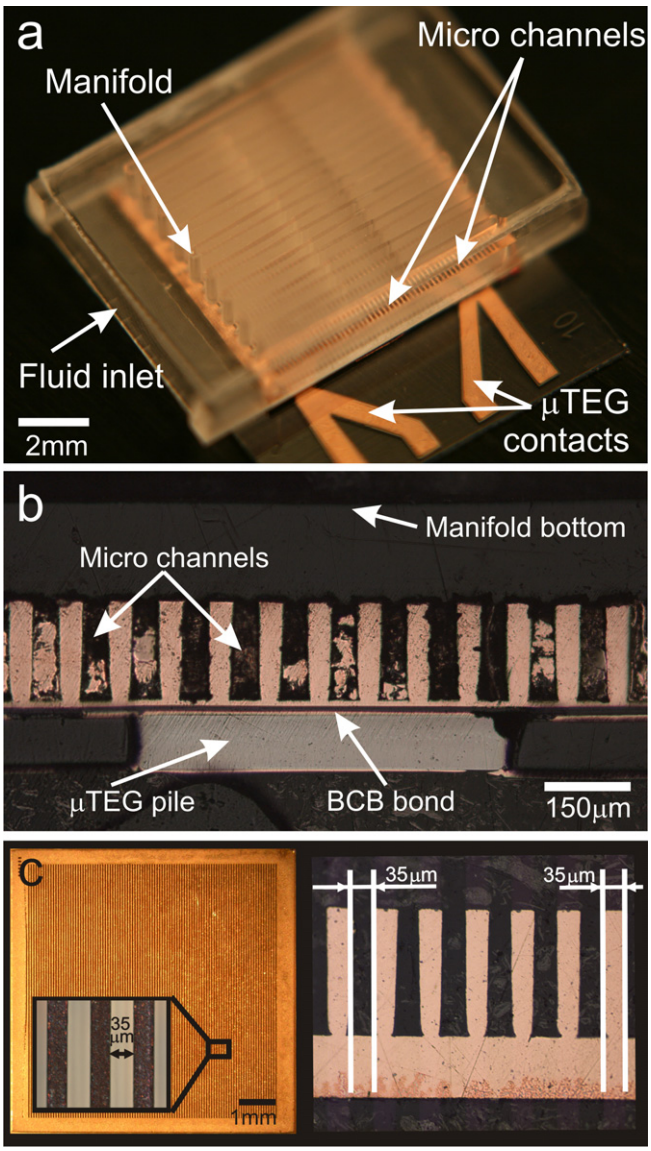

Fig. 4. Pictures of the assembled μHTS/μTEG stack (a) and cross-section view of a representative sample (b). The microchannels are filled with copper residues from the polishing process for cross-section preparation. Top-view of a microchannel chip and the corresponding cross section (c).

3. Experimental

The fabricated μHTS and μHTS/μTEG stack are characterized by heat flux, pressure drop and Seebeck voltage measurements in a fluid loop measurement setup. The devices are mounted on a temperature-controlled heat source, consisting of a resistive heater (platinum meander on Al_2O_3 substrate) and a BCB-bonded copper block for homogenous heat distribution (see inset in Figs. 5 and 6). The Cu block temperature is controlled with the help of an integrated thermocouple located at the center of the block. The surface area of the Cu block exposed to ambient air is kept small in order to reduce thermal losses through convection. Thus, the convective thermal losses are neglected. For an improved thermal interface between the Cu block and the heat sinks, a silicone thermal compound (k = 3.4 W/mK) is used and a constant pressure of 230 kPa applied. The heat flux through the device is assumed to be equivalent to the necessary heating power of the resistive heater in steady state condition. The cooling water (deionized) flow is controlled by a Coriolis flow meter (error: ±1% of reading) from 0.015 to 0.13 l/min. The water inlet temperature is kept at 293 ± 0.1 K. The applied temperature difference ΔT is calculated by subtracting the water inlet temperature from the controlled heater block temperature. The pressure drop over the heat sink is measured with a differential pressure sensor meter (error: ±2% of FS = 1 mbar). The heat flux and pressure loss measurements are sampled at a rate of 1.17 Hz and averaged over 3 min after reaching steady state condition. The μHTS performance is characterized by the achieved heat transfer resistance (R_{HS}) and the corresponding pumping power. The heat transfer resistance is calculated from the measured heat flux and the applied temperature difference ΔT. The pumping power is obtained from the resulting pressure drop over the heat sink and the applied volumetric flow rate.

For the μHTS/μTEG system characterization, the open circuit voltage of the μTEG is recorded as a function of the fluid flow rate and the applied temperature gradient. The relevant parameters of the μTEG used can be found in Table 1.

4. Results and discussion

4.1. Device fabrication

An assembled μHTS/μTEG system is depicted in Fig. 4a. The cooling liquid enters the manifold on the left hand side, flows

Table 1
Bi_2Te_3 μTEG parameters.

Seebeck voltage per TC (μV/K)	Efficiency ZT (–)	TEG output power (μW/K² cm²)	TEG resistance (Ω)	Total thickness (μm)	Thermal TEG resistance (cm² K/W)
102.3 ± 0.76	0.0164 ± 0.001	0.95 ± 0.0139	5.2 ± 6.12E–4	290 ± 7.1	9.13 ± 0.41

Table 2
Microchannels and manifold design parameters.

	Channel height (μm)	Channel width (μm)	Fin/channel wall width (μm)	Base height (μm)	Slot size (μm)	Total area (mm)
Cu microchannels	200	35	35	10	–	8 × 8
Manifold channels	1000	200–390 (tapered)	120	200	150	8.5 × 12

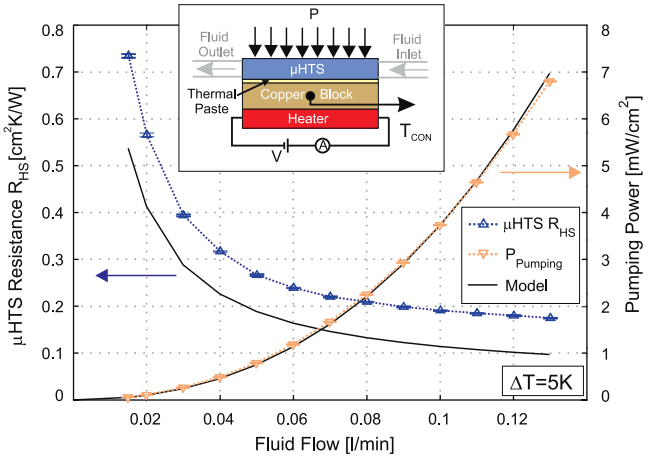

Fig. 5. Heat transfer resistance R_{HS} and corresponding pumping power measurements and calculations of the μHTS as a function of the fluid flow rate. The Cu block temperature was controlled to 298 ± 0.1 K. The error bars correspond to the standard deviations of the averaged signal over a measurement period of 180 s. The figure inset shows the schematics of the sample fixture in the measurement setup.

through the microchannels located underneath and exits the manifold on the opposite side. The device is connected to the fluid loop by a flexible tube at the fluid inlet and outlet. The relevant device parameters are summarized in Table 2. The dimensions of the μHTS were chosen to maximize the output power according to an extended thermal resistance model of the μHTS/μTEG stack

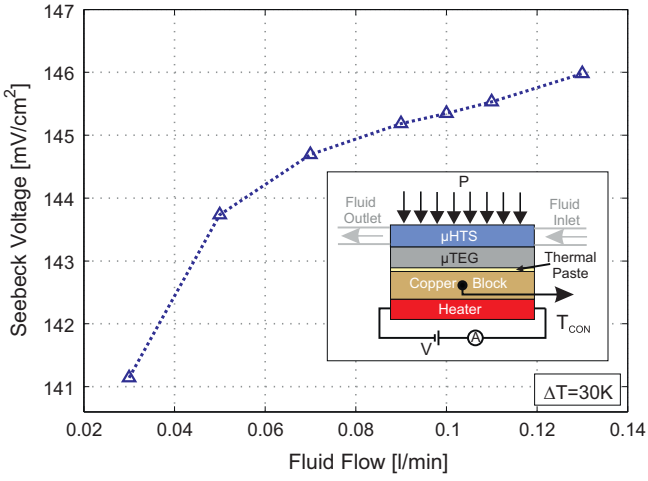

Fig. 6. Seebeck voltage measurements of the μHTS/μTEG stack as a function of the fluid flow rate at an applied ΔT of 30 ± 0.1 K. The error coming from random voltage fluctuations is below 0.1 mV/cm² (not included in graphic). The figure inset shows the schematics of the sample fixture in the measurement setup.

[10,15] while still complying with fabrication limits. Increasing the height of both channels would result in an improved hydrodynamic performance and reduced heat transfer resistance in the case of the microchannels, but would also complicate the fabrication process. Fig. 4b shows the cross section of the assembled stack with a Bi_2Te_3 μTEG pile, copper microchannel and a thin homogenous BCB bond layer in between. This bond interface also serves as electric isolation between the μTEG interconnects and the microchannel base. The depicted microchannels and the μTEG in Fig. 4b are taken from previously fabricated samples and do not correspond to the actual measured device. Fig. 4c shows the top view and a cross cut view of the used microchannels. The channels have an aspect ratio of 5.4 at a total height of 190 μm.

4.2. μHTS performance

The measured heat transfer resistance (R_{HS}) and corresponding pumping power with respect to the volumetric flow rate are plotted in Fig. 5. The applied flow rates of 0.015–0.13 l/min are in the relevant range for the characterization of the μHTS under investigation. The Cu block temperature was maintained at 298 ± 0.04 K. With rising flow rates, R_{HS} decreases due to an increase in the heat capacity rate of the fluid. The total thermal resistance of the μHTS is defined as

$$R_{HS} = R_{COND} + R_{CONV} + R_{HC} \quad (1)$$

where R_{COND} is the conductive resistance from the heater to the copper channel surface area, R_{CONV} the convective resistance and R_{HC} the fluid resistance due to its limited heat capacity. R_{HC} can be expressed as

$$R_{HC} = \frac{1}{\dot{m}c_p} = \frac{1}{\dot{v}\rho c_p} \quad (2)$$

where $\dot{m}$ is the mass flow rate, $\dot{V}$ the volumetric flow rate, ρ the fluid density and c_p the specific heat capacity. While the conductive and convective heat transfer resistances are nearly independent of the flow rate, R_{HS} decreases with increasing flow rates due to an increase in the effective thermal mass flow. At higher flow rates, the impact of the enhanced mass flow decreases and a further rise in the flow rate only marginally changes the total heat transfer resistance.

R_{COND} includes the thermal resistance of the copper channels as well as the interface losses between the Cu block and the μHTS. While the first can be neglected due to the high thermal conductivity of copper, the latter might include the effects of a thick silicone thermal compound or interface voids, resulting in a significant impact on the overall heat transfer resistance.

The pumping power in Fig. 5 increases with increasing fluid flow due to a rise in the hydrodynamic resistance with higher water flow. In the applied flow rate range (0.015–0.13 l/min), the calculated Reynolds number at the manifold channel inlet varies from 40 to

370 and 2 to 20 inside the microchannels, indicating a laminar flow regime.

The applied model in Fig. 5 is a semi-empirical one-dimensional model [18] extended with temperature dependent fluid parameters. The clear downward offset of the modeled R_{HS} with respect to the measurements indicate the above mentioned thermal losses between the Cu block and the μHTS (not included in the applied model). These thermal losses correspond to a silicone thermal compound thickness of approx. 26 μm. The computed pumping power is in good agreement with the experimental results.

Since the consumed power must be subtracted from the μTEG output power, a trade-off between the heat transfer resistance and the pumping power must be made. Depending on the specific applied temperature gradient and the μTEG parameters, an optimal fluid flow operating point will exist (will be discussed in Section 4.3).

4.3. μTEG/μHTS performance

The open circuit Seebeck voltage measurements as a function of the fluid flow rate through the μHTS are depicted in Fig. 6. With increasing fluid flow rates, the Seebeck voltage increases, following the inverse trend of the heat transfer resistance behavior (Fig. 5). However, it can be noticed that a rising fluid flow rate, i.e. decreasing R_{HS}, has a relatively small impact on the Seebeck voltage compared to the absolute measured value. The reason lies in the large difference between the thermal resistance of the μTEG (R_{TEG} = 9.13 cm² K/W) and the μHTS range (R_{HS} = 0.18–0.73 cm² K/W).

The Seebeck voltage of a TEG can be expressed as [19]

$$V = m\alpha\Delta T_{TEG} = m\alpha\frac{R_{TEG}}{R_{TEG}+R_{Contact}}T_{AMB} \quad (3)$$

where m is the number of the thermocouples, α the Seebeck coefficient of the thermoelectric material, ΔT_{TEG} the temperature gradient at the generator surface, $R_{Contact}$ the sum of the thermal contact resistances on the hot and cold sides and ΔT_{AMB} the ambient thermal gradient. In the system investigated here, ΔT_{AMB} is equal to the applied temperature gradient ΔT.

By introducing the ratio X between $R_{Contact}$ and R_{TEG} and assuming $m\alpha\Delta T_{AMB}$ to be a constant which is denoted by C, the equation can be simplified to

$$V = C\frac{R_{TEG}}{R_{TEG}+XR_{TEG}} = C\frac{1}{1+X} \quad (4)$$

With decreasing X, i.e. decreasing $R_{Contact}$, the Seebeck voltage will increase. At $X \ll 1$, i.e. $R_{TEG} \gg R_{Contact}$, and small variations of $R_{Contact}$ with respect to R_{TEG}, the impact on V will be minor.

The same applies for the output power P_{OUT} of a μTEG. In a simplified thermal resistance model, P_{OUT} can also be described as [20]

$$P_{OUT} = C^*\frac{R_{TEG}}{(R_{TEG}+R_{Contact})^2} = C^*\frac{1}{R_{TEG}(1+X)^2} \quad (5)$$

with

$$C^* = \frac{\Delta T_{AMB}^2\eta_{TE}}{T\eta_C} \quad (6)$$

where T is the mean temperature of the system, η_C the Carnot and η_{TE} the thermal efficiency of the thermoelectric generator.

By reducing $R_{Contact}$, the output power of the generator will be increased for arbitrary R_{TEG}. Additionally, for a fixed $R_{Contact}$, the maximum of the equation is reached, when R_{TEG} is equal to $R_{Contact}$. Therefore, by decreasing R_{TEG} (by e.g. reducing the generator's thickness) to match the $R_{Contact}$, the impact of the small R_{HS} can be better exploited and the output power can be further

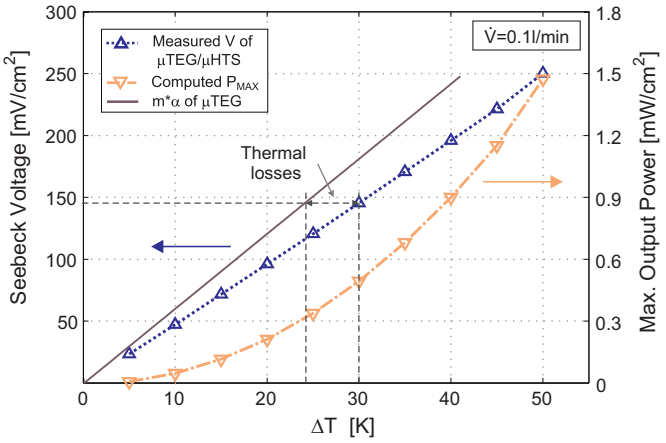

Fig. 7. Seebeck voltage measurements and maximum output power of the μHTS/μTEG stack as a function of applied temperature gradient at a fluid flow rate of 0.1 l/min. The error coming from random voltage fluctuations is below 0.1 mV/cm² (not included in graphic).

enhanced. However, in real applications, practical limits of maintaining the temperature gradient ΔT_{AMB} with small R_{TEG} exist and must be considered for the system design.

In Fig. 7, the measured Seebeck voltage and the corresponding calculated μTEG output power is plotted versus the applied temperature gradient. A fluid flow rate of 0.1 l/min was selected to explain the dependence of the Seebeck voltage on ΔT for a characteristic working point. The solid line represents the Seebeck voltage resulting from the previously characterized Seebeck coefficient of the thermocouples (see Table 1). At a specific Seebeck voltage, the actual temperature gradient at the surface of the generator can be determined (see vertical dashed line in Fig. 7). Assuming that an equal heat flux runs through the generator at the same measured Seebeck voltage, the total thermal contact resistance between the reservoirs of the cold and hot sides is calculated to be 2.27 ± 0.13 cm² K/W (at ΔT = 30 K). By subtracting the corresponding R_{HS} of 0.19 ± 1E−3 cm² K/W (see Fig. 5 at a fluid flow rate of 0.1 l/min), the thermal interface losses are estimated to be 2.08 ± 0.13 cm² K/W. This relatively high value mainly results from the insufficient thermal coupling between the generator and the heater block, since the μTEG surface is not totally flat and contains some defects and voids.

The maximum output power is computed from the measured Seebeck voltage and the electrical resistance of the μTEG (see Table 1) assuming matched load conditions [15,21]. A maximum power of 1.47 mW/cm² is reached at an applied temperature difference of 50 K. At this high flow rate of 0.1 l/min and thus high pumping power of 3.74 mW/cm², no positive net output power can be achieved with the low ZT values of the μTEG used.

In order to predict the potential performance of the presented μHTS/μTEG system, the measured μHTS parameters and improved μTEG thermoelectric material properties are inserted into the model of Fig. 1.

The μHTS parameters inserted into the model are selected in order to maximize the computed net output power for an applied temperature gradient of 0–65 K. A heat transfer resistance of 0.74 ± 6E−3 cm² K/W at a fluid flow rate of 0.015 l/min is used and the corresponding measured pumping power of 0.073 ± 1E−3 mW/cm² is subtracted from the μTEG output power. The estimated thermal interface losses between heater and device are also included in the model. The simulated output power as a function of the applied temperature gradient and different ZT values is plotted in Fig. 8.

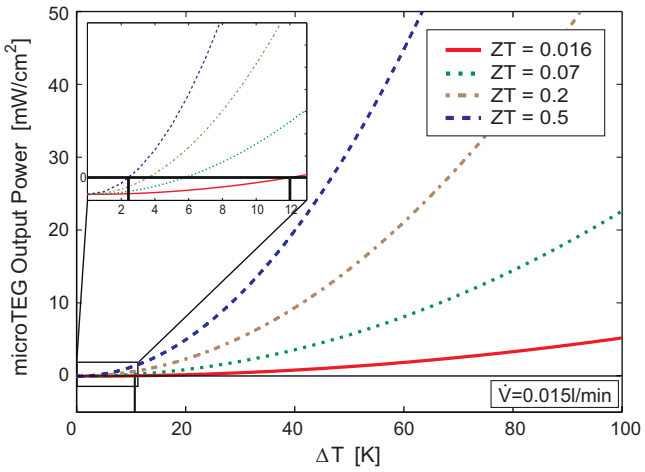

Fig. 8. Simulated Bi_2Te_3 μTEG (R_{TEG} = 9.13 cm² K/W) output power dependence on the applied temperature gradient and different *ZT* values. A heat transfer resistance of 0.74 cm² K/W and a pumping power of 0.073 mW/cm² were used, corresponding to a μHTS fluid flow of 0.015 l/min. The cold side temperature is set to 293 K.

The optimal operating point for this μHTS/μTEG configuration and boundary conditions is at a low flow rate, since the increase of the required pumping power overweighs the limited impact of the reduced R_{HS} at higher flow rates. By decreasing R_{TEG} (i.e. increasing the ratio of R_{HS} to R_{TEG}) and the interface contact resistance to the heater, the influence of a small R_{HS} will increase and the optimal operating point will shift to larger fluid flows.

The continuous red line in Fig. 8 represents the power output of the μHTS/μTEG stack for the *ZT* of the generator used (see Table 1). A positive net power can be reached at a temperature gradient of ~12 K. By increasing the *ZT* to a state-of-the-art value of 0.5 for Bi_2Te_3, a positive output power starting from an applied ΔT of ~2.5 K could be achieved.

5. Conclusions

A new microfluidic packaging approach for the power enhancement of μTEGs is presented. The two level heat transfer system consists of high aspect ratio copper microchannels for efficient heat dissipation and a polymer manifold fluid distribution layer for a reduced hydrodynamic resistance.

The fabrication process of the μHTS and the integration with a μTEG were successfully demonstrated. The fabricated prototype was characterized by heat flux, pressure losses and Seebeck voltage measurement in a controlled fluid loop. The μHTS achieved a heat transfer resistance of 0.74 cm² K/W at a very low pumping power of 0.073 mW/cm². Further, a maximum μTEG output power of 1.47 mW/cm² was reached at an applied temperature difference of 50 K and a fluid flow rate of 0.1 l/min (3.74 mW/cm² pumping power).

The complete system can be further optimized, by reducing the μTEG thickness and interfacial thermal losses. Simulations based on the measured system parameters but with a state-of-the-art *ZT* value of 0.5 for Bi_2Te_3, show a net output power gain starting from an applied temperature gradient as low as 2.5 K.

Acknowledgements

The authors would like to thank GreenTEG for providing the μTEG sample, ETH Zurich for the financial support, Lukas Rüthemann for his help with the measurements and the mechanical workshop D-PHYS for fabricating the manifold channels.

References

[1] R. Venkatasubramanian, E. Siivola, T. Colpitts, B. O'Quinn, Thin-film thermoelectric devices with high room-temperature figures of merit, Nature 413 (2001) 597–602.
[2] T.C. Harman, M.P. Walsh, B.E. Laforge, G.W. Turner, Nanostructured thermoelectric materials, J. Electron. Mater. 34 (2005) L19–L22.
[3] W. Glatz, E. Schwyter, L. Durrer, C. Hierold, Bi_2Te_3-based flexible micro thermoelectric generator with optimized design, J. Microelectromech. Syst. 18 (2009) 763–772.
[4] V. Leonov, T. Torfs, P. Fiorini, C. Van Hoof, Thermoelectric converters of human warmth for self-powered wireless sensor nodes, IEEE Sens. J. 7 (2007) 650–657.
[5] J.H. Yang, F.R. Stabler, Automotive applications of thermoelectric materials, J. Electron. Mater. 38 (2009) 1245–1251.
[6] D.T. Crane, G.S. Jackson, Optimization of cross flow heat exchangers for thermoelectric waste heat recovery, Energy Convers. Manage. 45 (2004) 1565–1582.
[7] B. Agostini, M. Fabbri, J.E. Park, L. Wojtan, J.R. Thome, B. Michel, State of the art of high heat flux cooling technologies, Heat Transfer Eng. 28 (2007) 258–281.
[8] R.H.W. Pijnenburg, R. Dekker, C.C.S. Nicole, A. Aubry, E.H.E.C. Eummelen, Integrated micro-channel cooling in silicon, in: ESSDERC 2004: Proceedings of the 34th European Solid-State Device Research Conference, 2004, pp. 129–132.
[9] D.B. Tuckerman, R.F.W. Pease, High-performance heat sinking for Vlsi, Electron. Device Lett. 2 (1981) 126–129.
[10] W. Escher, D. Poulikakos, T. Brunschwiler, B. Michel, Experimental investigation of an ultrathin manifold microchannel heat sink for liquid-cooled chips, J. Heat Trans.: Trans. ASME 132 (2010).
[11] E.G. Colgan, B. Furman, M. Gaynes, N. LaBianca, J.H. Magerlein, R. Polastre, R. Bezama, K. Marston, R. Schmidt, High performance and subambient silicon microchannel cooling, J. Heat Trans.: Trans. ASME 129 (2007) 1046–1051.
[12] L. Boteler, N. Jankowski, B. Geil, P. McCluskey, A micromachined manifold microchannel cooler, in: IMECE2009: Proceedings of the ASME International Mechanical Engineering Congress and Exposition, vol. 5, 2010, pp. 61–68.
[13] G.P. Peterson, C.S. Chang, Two-phase heat dissipation utilizing porous-channels of high-conductivity material, J. Heat Trans.: Trans. ASME 120 (1998) 243–252.
[14] T. Brunschwiler, H. Rothuizen, M. Fabbri, U. Kloter, B. Michel, R.J. Bezama, G. Natarajan, Direct liquid jet-impingement cooling with micron-sized nozzle array and distributed return architecture, 2006, in: Proceedings 10th Intersociety Conference on Thermal and Thermomechanical Phenomena in Electronics Systems, vols. 1 and 2, 2006, pp. 196–203.
[15] M. Strasser, R. Aigner, C. Lauterbach, T.F. Sturm, M. Franosch, G. Wachutka, Micromachined CMOS thermoelectric generators as on-chip power supply, Sens. Actuator A: Phys. 114 (2004) 362–370.
[16] C.D. Joye, J.P. Calame, M. Garven, B. Levush, UV-LIGA microfabrication of 220 GHz sheet beam amplifier gratings with SU-8 photoresists, J. Micromech. Microeng. 20 (2010).
[17] J. Zhang, W.X. Zhou, M.B. Chan-Park, S.R. Conner, Argon plasma modification of SU-8 for very high aspect ratio and dense copper electroforming, J. Electrochem. Soc. 152 (2005) C716–C721.
[18] W. Escher, D. Poulikakos, B. Michel, A novel high performance, ultra thin heat sink for electronics, Int. J. Heat Fluid Fl. 31 (2010) 586–598.
[19] W. Glatz, S. Muntwyler, C. Hierold, Optimization and fabrication of thick flexible polymer based micro thermoelectric generator, Sens. Actuators A: Phys. 132 (2006) 337–345.
[20] J.W. Stevens, Optimal design of small ΔT thermoelectric generation systems, Energy Convers. Manage. 42 (2001) 709–720.
[21] D.M. Rowe, G. Min, Peltier devices as generators, in: D.M. Rowe (Ed.), CRC Handbook of Thermoelectrics, CRC Press, Boca Raton, London, 1995.

Biographies

N. Wojtas studied at the department of Mechanical and Process Engineering at ETH Zürich, where she received her bachelor degree in Mechanical Engineering and the MSc in Micro and Nanosystems. She completed a 4 months internship in DENSO research Laboratories in Nisshin, Japan, where she worked on micro optical devices. Her Master Thesis focused on the development of new fabrication methods for flexible micro thermoelectric generators and was carried out in Micro and Nanosystems group at ETH Zurich. She remained in the group as a Ph.D. student to continue the research in the field of thermoelectric energy harvesting.

E. Schwyter studied at the department of Electrical Engineering and Information Technology at the ETH Zurich, where he received his MSc in Electrical Engineering. His main focuses have been Biomedical Engineering and Microsystems Technology. He carried out his Master Thesis at the University of Calgary, Canada, in the field of multimodal microMRI and microCT 3D imaging. During 4 month he worked at Micronova, the Centre for Micro and Nanotechnology in Espoo, Finland, where he focused on the optimization of plasma ashing and oxidation as well as lift-off processes. He joined the Micro and Nanosystems group at ETH Zürich as a PhD student to investigate the further development and optimization of micro thermal generators. Besides his PhD he co-founded greenTEG GmbH, an ETH SpinOff company focused on the commercial fabrication of electroplated thermoelectric devices.

W. Glatz received his PHD degree from ETH Zurich in 2008. Since 2009 he is the CEO of greenTEG, a start-up company, focusing on the development and commercialization of thermoelectric generators. Previously he was a postdoctoral research

scientist at IBM's Zurich Research Lab working on thermal interfaces, packaging, liquid cooling and solar concentrator technology. He has studied with several international institutions including the Universidad Politecnica de Valencia, Spain, the University of Oklahoma, USA and the Technical University of Braunschweig, Germany where he received his Diploma Degree in Mechanical Engineering in 2002.

S. Kühne studied mechanical engineering at ETH Zurich with focus in micro-/nanosystems and control technology. He carried out his diploma thesis with Sensirion AG. The thesis research included the development of a CMOS-compatible wafer-level fabrication process for microhotplate-based gas sensors as well as the characterization of the fabricated devices. Currently, his main field of research as a PhD student within the Micro and Nanosystems group at ETH Zurich is focused on active electrostatic micro bearings for application in MEMS gyroscopes.

W. Escher joined the Advanced Packaging Group as a PhD student in 2006. He received his doctorate in 2009 from Swiss Federal Institute of Technology (ETH) in the area of micro- to nanoscale heat and mass transfer. In the scope of his thesis he explored the potential of so called nanofluids for electronics cooling and developed a high efficiency micro-fluidic heat sink with an incorporated hierarchical fluid supply network. Currently he is a Research Staff Member at the IBM Zurich Research Laboratory. His research interests include single–phase cooling, thermal interfaces, novel packaging techniques for high powered thermal-fluidic microelectronic packages and high concentrating photovoltaic systems.

C. Hierold is Professor for Micro- and Nanosystems at ETH Zurich since April 2002. Before, he was eleven years with Siemens AG, Corporate Research, and Infineon Technologies AG in Munich, Germany, working mainly on CMOS compatible microsystems. His major research at ETH Zurich is now focused on the field of nanotransducers, evaluation of new materials for MEMS and advanced microsystems. Christofer Hierold has been serving in program committees of numerous scientific conferences; he is co-chair of the Steering Committee of the European Conference on Solid-State Transducers (Eurosensors) and he is member of the Steering Committee of the International Conference on Solid-State Sensors, Actuators and Microsystems (Transducers). He is active as subject editor of the IEEE/ASME Journal of Micro Electromechanical Systems, JMEMS, and member of the editorial Board of the IOP Journal of Micromechanics and Microengineering, JMM.